Soft Matter

View Online
Dynamic Article Links

Cite this: *Soft Matter*, 2011, **7**, 7976

www.rsc.org/softmatter

COMMUNICATION

Substrate dependent drop deformation and wetting under high frequency vibration

Ofer Manor, Michael Dentry, James R. Friend and Leslie Y. Yeo*

Received 6th June 2011, Accepted 8th July 2011
DOI: 10.1039/c1sm06054f

We explore the peculiar steady component of a sessile drop response to MHz order vibration, found to be dependent on its initial wettability. Placed on a vibrating hydrophobic substrate, the drop elongates vertically in the direction of the incident sound wave while remaining hydrophobic. In contrast, the drop is seen to spread on a slightly hydrophilic substrate. We elucidate this discrepancy by revealing the competing effects between the radiation pressure exerted at the bulk air/water interface and the acoustic streaming force on the contact line, revealing the critical role of the flow in the viscous boundary layer.

While a number of interesting phenomena pertaining to vibration-induced liquid spreading, such as climbing drops,[1] transition to superhydrophobicity,[2] liquid contour oscillation,[3] *etc.*, have been reported, there have been few fundamental studies explaining wetting effects under *high frequency* (MHz order) vibration despite renewed interest in acoustically-driven microfluidic drop actuation.[4,5] Here, we investigate MHz frequency pistonlike vibration of a sessile drop, a rather simple experiment but one that reveals an interesting characteristic—the drop response has a steady component that behaves very differently depending on its initial wettability. There have only been attempts to explore the behavior of vibrated liquid drops and films excited up to tens of kHz to date;[6,7] the observations we report here, and elucidate with a fundamental theoretical model, were seemingly absent from these earlier experiments due to a key factor—at 10 kHz order, acoustic streaming within the viscous boundary layer is negligible.[7] For simplicity, we will limit our discussion to the steady deviation of the drop shape from its equilibrium state at rest and ignore fast fluctuations—a reasonable assumption given that *the drop shape transitions and contact line dynamics occur on much longer time scales than that of the excitation or the drop oscillation*. The qualitative agreement between the experiments and theoretical prediction, which allow for boundary layer streaming effects, suggest they play a fundamental role in the peculiar response observed.

Two μl deionized water drops (Millipore, Billerica, MA) were dispensed onto a 20 mm diameter and 0.99 mm thick lead zirconate titanate (PZT) thickness polarized disk (C-203; Fuji Ceramics Corp., Tokyo, Japan), on which a thin film of polytetrafluoroethylene (PTFE) (Teflon® 60151-100-6; Dupont, Wilmington, DE) or polydimethylsiloxane (PDMS) (Sylgard 184; Dow Corning, Midland, MI) was coated (Fig. 1 inset). We spin coated PTFE on the disk at 50 rpm for 10 s and then at 500 rpm for 60 s, followed by baking at 250 °C for 2 h. Another disk was dip-coated in a PDMS solution consisting of 0.4 g silicone elastomer base and 0.1 g curing agent dissolved in 10 ml toluene (601-021-00-3; Merck KGaA, Darmstadt, Germany). The coated disk was then kept at room temperature for 3 days over which the solvent slowly evaporated and subsequently baked at 70 °C for 2 h to allow final curing of the polymer. To drive disk vibration, we applied an electrical signal at resonance (2.23 and 2.11 MHz for the PTFE and PDMS coated disks, respectively) using a signal generator (SML01; Rhode & Schwarz, North Ryde, NSW, Australia) and amplifier (10W1000C;

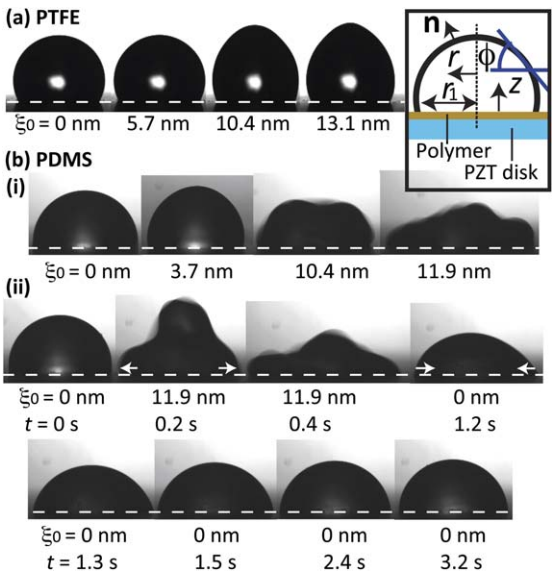

Fig. 1 Response of a 2 μl drop atop a PZT disk coated with (a) PTFE or (b-i) PDMS, under varying vibration amplitudes ξ_0. The initially pinned contact line becomes unpinned for $\xi_0 > 5.8$ nm (PTFE) and $\xi_0 > 3.7$ nm (PDMS). (b-ii) Time series plot of the drop atop PDMS illustrated in (b-i) showing the initially spreading drop ($0 < t < 0.4$ s) subsequently receding to its initial position as the power is relaxed ($t > 1.2$ s); the arrows show the contact line displacement direction. After spreading to its equilibrium position, the contact line continues to vibrate but without any net displacement at long times. Inset: Schematic of the experimental setup; the dashed line denotes the symmetry axis.

Micro/Nanophysics Research Laboratory, Monash University, Clayton, VIC, 3800, Australia. E-mail: leslie.yeo@monash.edu

Amplifier Research, Souderton, PA), where the top face electrode was grounded to avoid electric field effects within the drop; an oscilloscope (Wavejet 332/334; LeCroy, Chestnut Ridge, NY) was used to measure the power input to the disks. Prior to each measurement, the drop was vibrated to eliminate air pockets from the substrate/water interface. The disk temperature was measured before and after each run; we also observed the variation in drop mass to be around 10%, and evaporative losses were found to be less than 1% over the 5–6 s run duration. The drop shape was acquired using high speed imaging (MC1310, Mikrotron GmBH, Unterschleissheim, Germany) at 1600 fps. The apparent contact angle θ was determined through visual inspection of the magnified drop images and averaging 20–40 repeated images over two oscillation periods. We measured the surface vibration half-amplitude ξ_0 using a laser doppler vibrometer (UHF-120; Polytec GmBH, Waldbronn, Germany), where each datapoint is an average of 49 measurements over a 2 × 2 mm disk area. The water surface tension, viscosity and density are $\gamma = 72$ mN m^{-1}, $\mu = 0.89$ mPa s and $\rho = 1000$ kg m^{-3}, respectively.

Fig. 1(a) shows a drop atop PTFE with initial contact angle $\theta_0 = 120°$. The drop is observed to progress through three distinct stages as ξ_0 is increased. At low ξ_0, the contact line remains pinned and the interface deforms vertically in the direction of the incident sound beam. Above a threshold, the contact line unpins and the average contact angle θ is seen to decrease while remaining hydrophobic ($90° < \theta < \theta_0$). The drop continues to deform vertically but retains a stable shape as shown. Upon increasing ξ_0 further, the interface is observed to oscillate more rapidly until a second threshold is crossed, above which the interface becomes unstable and breaks-up.[8]

Atop PDMS ($\theta_0 = 88°$), the drop progresses through three similar stages (Fig. 1(b-i)). Initially the drop deforms vertically while the contact line is pinned. Above a ξ_0 threshold value the contact line then unpins. The unpinned contact line is, however, observed to advance rapidly such that the drop spreads over the substrate. Interfacial and contact line oscillations are considerable and although it is clear that the drop has spread, it does not retain a well-defined shape as with the drop atop PTFE. This is attributed to the increased drop wetting area during spreading that increases the mechanical power transmitted into the drop. The spreading dynamics is shown in Fig. 1(b-ii): while the drop and contact line fluctuate continuously, the drop initially bulges upwards and then spreads such that the contact line is displaced outwards to a point where it simply vibrates around this new equilibrium position ($t > 0$ s, $\xi_0 = 11.9$ nm). When the vibration is relaxed ($t > 1.2$ s, $\xi_0 = 0$), the contact line recedes back to its initial position; consequently, the drop slowly retracts to its equilibrium hemispherical shape at rest. The contact line dynamics occurs over a much longer time scale (O(1 s)) compared to that of the substrate vibration (O(10^{-6} s)) and the drop's oscillatory response (O(10^{-6}–10^{-2} s)), and hence our observations are not directly related to the contact line fluctuations.

We now formulate simple models to describe this discrepancy. It is instructive to note that the sound wavelength in the drop generated by the MHz vibration is shorter than the drop dimension. This gives rise to two dominant phenomena in the drop: an interfacial acoustic radiation pressure as the sound wave impacts the interface due to the air/water acoustic impedance mismatch, and the attenuation of the sound waves in the drop accompanied by flow within the *bulk* of the drop (Eckart streaming) and in a *viscous boundary layer* immediately above the substrate. The radiation pressure is expected to deform the drop vertically (see schematic in Fig. 2), whereas the rapid boundary layer rotational flow is expected to drive drop spreading; bulk streaming will be shown to have a negligible effect on the interface dynamics below.

The dimensionless normal stress balance across the interface in axisymmetric polar coordinates (r, 0, z) reads

$$(1/\tilde{R}_1 + 1/\tilde{R}_2) = \tilde{p} + \mathrm{Bo}\tilde{z} - \mathrm{We}\tilde{p}_r, \quad (1)$$

where R_1 and R_2 are the principal radii of curvature of the drop, p is the Laplace pressure, determined from mass conservation, and p_r the acoustic radiation pressure; the tilde decoration denotes dimensionless quantities, obtained using the following transformation: $(\tilde{R}_1, \tilde{R}_2, \tilde{z}) \equiv (R_1, R_2, z)/R$ and $\tilde{p} = (R/\gamma)p$, wherein R is the drop characteristic length scale, which we take to be the radius of a spherical drop. We neglect the viscous stress induced by Eckart streaming since the streaming velocity $u_c \approx \xi_0\omega \sim 10^{-2}$ m s^{-1} (wherein ω denotes the angular vibration frequency) gives rise to a viscous normal stress $\mu u_c/R \sim 10^{-2}$ Pa that is far smaller than the characteristic Laplace pressure $\gamma/R \sim 10^2$ Pa. We note the inclusion of two additional terms in eqn (1) involving gravitational effects, captured through the Bond number $\mathrm{Bo} \equiv \rho g R^2/\gamma$, and the acoustic radiation pressure, quantified by an acoustic Weber number $\mathrm{We} \equiv \rho R(\omega\xi_0)^2/\gamma$; g is the the gravitational acceleration. The incident traveling sound wave, generated by the disk vibration $\xi = \xi_0 \sin \omega t$, satisfies the velocity field $u_z\hat{z} = \omega\xi_0\cos[(2\pi z/\lambda) - \omega t]$,[9] where λ is the wavelength; attenuation and dissipative effects are assumed negligible. The incident *traveling* wave is subsequently reflected from the interface (assumed completely) as $u_x\hat{x}$ ($\hat{x}$ being a function of the local interfacial curvature $\nabla\cdot\mathbf{n}$ on reflection), such that $\mathbf{u} = u_z\hat{z} + u_x\hat{x}$. Wave reflection then results in the radiation pressure $\mathbf{p_r} = p\mathbf{I}\cdot\mathbf{n} + \langle\rho\mathbf{uu}\cdot\mathbf{n}\rangle$; p denotes the local excess hydrostatic pressure due to compressional effects and $\mathbf{I}$ is the identity tensor; the parenthesis $\langle\cdot\rangle$ signifies a time average of the inner quantity over the acoustic period.[9–11] The local excess hydrostatic pressure may be approximated as $p \approx (B/2A)\langle E\rangle$,[12] quantifying the local isotropic contribution of the acoustic energy density E to $\mathbf{p_r}$; B/A is a parameter that describes the nonlinearity of the acoustic wave.[13] Additional contributions to $\mathbf{p_r}$ due to transient perturbations of the interface may be ignored to first approximation.[11] The dimensionless normal component of the radiation pressure in eqn (1) then becomes $\tilde{p}_r = \mathbf{p_r}/2E \approx \mathrm{B}/4A + \cos^2\phi$, where $E \approx \rho(\omega\xi_0)^2/2$.

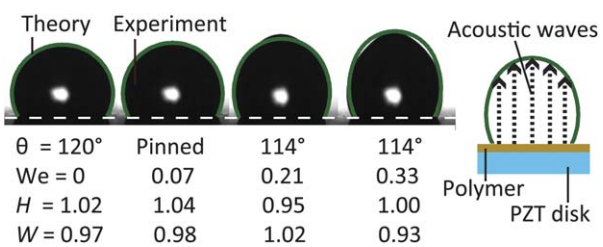

Fig. 2 Comparison between theory (eqn (1)) and experiment for a water drop atop a PTFE coated PZT disk (shown also in Fig. 1(a)), where Bo = 0.085. ξ_0 (and hence We) and θ are measured values; pinned refers to the contact line. H and W are the theoretical to experimental ratios of the drop height and wetted area, showing the agreement between the prediction and experiment. The schematic illustrates the incident acoustic waves, generated by the PZT disk, propagating upwards and impinging the drop interface.

To account for deviations of the equilibrium contact angle due to streaming effects, eqn (1) is solved numerically subject to boundary conditions that impose contact line pinning or specify the apparent contact angle θ. We note that θ may assume an arbitrary value within the contact angle hysteresis range.[14] The solution method is described elsewhere.[15] The quasi-static drop deformation model described by eqn (1) requires the implicit assumption that the drop reaches a steady-state over time scales far longer than the characteristic oscillation period, not unreasonable given the high vibration frequencies. At sufficiently high power levels, however, the nonlinear generation of sound frequencies closer to the drop fundamental frequency (O(0.1–1 kHz))[8] gives rise to apparent transient oscillations, as shown, for example, in Fig. 1(b). Fig. 2 shows a comparison between the theoretical quasi-static drop shape and the experiment for the drop atop the PTFE layer. The agreement, at least at vibration amplitudes of O(10 nm) and accelerations of O(10^4 m s^{-2}) in which transient drop oscillations are minimal such that a quasi-static model suffices, demonstrates the role of the acoustic radiation pressure in deforming the drop. In particular, the vertical propagation of a sound beam, generated by the pistonlike vibration of the substrate, can only deform the drop upwards. Despite the simple equilibrium theory invoked, we observe decent agreement between the prediction and the experiment for the drop response above PTFE, seen by the theoretical to experimental ratios of the drop height H and wetted area W in Fig. 2 which are close to unity. A different force arising from the flow in the boundary layer is nevertheless responsible for the contact line displacement observed for the drop atop PDMS (Fig. 1(b)).

We thus turn our attention to a scaling model that captures this contact line force. A quasi-static equilibrium force balance is invoked, justified given the much shorter MHz oscillation period compared to the spreading time scale. A distinct difference from eqn (1), however, is that we now conduct a balance of the *surface* forces at the contact line as opposed to along the interface of the *bulk* of the drop. As depicted in the inset in Fig. 3, the modified Young equation then reads

$$\gamma\cos\theta + \gamma_{sl} - \gamma_{sv} = F, \tag{2}$$

where γ_{sl} and γ_{sv} is the surface tension at the water/substrate and air/substrate interfaces, respectively. The existence of an additional tension at the contact line F that is balanced by the existing surface forces and that alters the equilibrium contact angle θ from its initial contact angle θ_0 is reminiscent of that in static electrowetting,[16,17] and is justified if the interfacial stress, imposed by the vibrating substrate, is localized within a small region at the contact line such that it is possible to average the stress over this region to obtain a finite net force density that acts at the contact line,[16,17] as shown below.

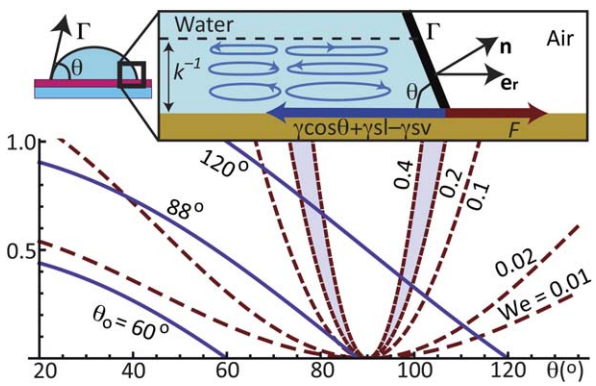

Fig. 3 Graphical solution of eqn (4) for a 2 μl drop. Solid lines represent the left side of eqn (4) for different θ_0 and dashed lines represent the right side for different We—intersections therefore constitute solutions; the shaded area shows the solution domain for the range of We used. Inset: Schematic illustration of the viscous boundary layer in the vicinity of the interface Γ and the force balance at the three-phase contact line.

A likely candidate is the momentum transfer that arises from the rotational component of the vibration-driven flow field $\mathbf{u}_t$, confined within a boundary layer of thickness $k^{-1} \equiv \sqrt{2\mu/\rho\omega} \simeq 0.4$ μm in a manner analogous to Schlichting streaming.[18] Mass and momentum conservation requires $\nabla\cdot\mathbf{u}_t = 0$ and $\partial\mathbf{u}_t/\partial t = -\mu(\nabla\times\nabla\times\mathbf{u}_t)/\rho$. Assuming the z-component of $\mathbf{u}_t$ follows $u_{tz} = A\exp[i(k'z - \omega t)]$,[9] continuity requires $u_{tr} = (C/r) - (iAk'r/2)\exp[i(k'z - \omega t)]$, where A is the velocity amplitude, k' a complex wave number and C a constant. Momentum conservation then specifies $k' = (-1)^{1/4}k$. Imposing the kinematic and no-slip conditions on the substrate, $u_{tz} = \xi_0\omega\cos(\omega t)$ and $u_{tr} = 0$ at $z = 0$, respectively, it follows that $u_{tz} = \omega\xi_0[e^{-kz}\cos(kz - \omega t) + e^{kz}\cos(kz + \omega t)]/2$ and $u_{tr} = \omega\xi_0 kr[e^{-kz}H(kz - \omega t) - e^{kz}H(kz + \omega t)]/4$, where $H(a) = \cos a + \sin a$ for the velocity field to be finite. The first term on the right of u_{tz} and u_{tr} propagates in the $+z$ half space and the second term, an image source invoked from symmetry considerations to satisfy no-slip, propagates in the $-z$ half space. The amplitude of u_{tz} is thus half the excitation amplitude as a result of the friction between the drop and the substrate, captured by the no-slip condition and the image solution.

We proceed by seeking an approximate solution for the boundary layer flow $\hat{\mathbf{u}}_t$ along the interface Γ (Fig. 3 inset). Since the boundary layer flow is not associated with the pressure distribution to first approximation, the interface does not deform and hence $\hat{\mathbf{u}}_t\cdot\mathbf{n} = 0$ at Γ. Further, since the interface cannot sustain tangential stresses, *i.e.*, $\partial\hat{\mathbf{u}}_t/\partial\mathbf{n} = 0$ on Γ, we approximate the interfacial flow as $\hat{\mathbf{u}}_t \approx \mathbf{u}_t\cdot(\mathbf{I} - \mathbf{nn})$ at Γ. Integrating the approximate radial Reynolds stress from the contact line (Γ = 0) over the entire boundary layer, the radial force per unit length along the contact line yields

$$F = \int_{\Gamma=0}^{\infty} \left\langle \left(\rho\hat{\mathbf{u}}_t\hat{\mathbf{u}}_t\cdot\mathbf{e_r}\right)\cdot\mathbf{e_r}\, d\Gamma\right\rangle \approx \rho k(\omega\xi_0 r_1)^2\cos^2\theta/32, \tag{3}$$

where $\mathbf{e_r}$ denotes the radial unit vector. Eqn (3) excludes $O(k^{-1}/R)$ contributions and assumes $r \approx r_1$, where r_1 denotes the radial length of the substrate/drop interface as shown in the inset of Fig. 1, and that the interface inclination is constant ($\phi \sim \theta$). Since the interfacial flow is approximated from an unbounded flow field, we expect an overprediction of the force imposed on the contact line. Substituting eqn (3) into eqn (2) then gives an approximate condition for the contact angle:

$$\cos\theta - \cos\theta_0 = \frac{\tilde{r}_1^2}{32}\mathrm{We}\cos^2\theta, \tag{4}$$

where $\tilde{r}_1 = r_1/\sqrt{k^{-1}R}$ and $\cos\theta_0 = (\gamma_{sv} - \gamma_{sl})/\gamma$, with γ_{sv} and γ_{sl} being the substrate/air and substrate/drop tensions, respectively; the substrate is assumed to be homogeneous such that a unique value of θ_0 can be specified.

Fig. 3 shows a representation of eqn (4) for a 2 μl drop for different We and θ_0. Valid solutions require the sum of the surface forces $\gamma\cos\theta + \gamma_{sl} - \gamma_{sv}$ on the left of eqn (4), denoted by the solid lines, to balance the additional acoustic tension F on the right of eqn (4), denoted by the dashed lines. We observe hydrophobic and hydrophilic solution branches for θ for drops on hydrophobic

substrates ($\theta_0 \geq 90°$) for all We. For given $\theta_0 \geq 90°$, the hydrophobic solution branch ($\theta_0 \geq 90°$) is closer to the initial value and thus θ is more likely to assume this value. This is qualitatively observed in our experiment for the drop atop PTFE (Fig. 1(a)), where We = 0–0.3. We note that eqn (4) slightly overpredicts the equilibrium contact angles—$\theta_0 \simeq 90°$ and 98° compared to experimental measurements of 114° at 124 and 196 mW, respectively. For initially hydrophilic substrates ($\theta_0 < 90°$), one has to traverse the solution space for small We to obtain solutions. The absence of solutions over the experimental We range for unpinned contact lines (We = 0.2–0.3; shaded area in Fig. 3) suggests the drop hypothetically spreads into a thin wetting film ($\theta = 0°$). It is clear, however, that the drop atop the PDMS layer (Fig. 1(b)) only spreads over a finite length to a point where $\theta \ll 90°$ —possibly because the theory above overpredicts the acoustic contribution F and does not account for the effect of disjoining pressure and the substrate roughness that impose additional energy barriers to the displacement of the contact line (through hysteresis in the contact angle).[19] Nevertheless, the contact angle condition given by eqn (4) affords valuable physical insight into the curious dependence of the vibrated drop shape on its initial wettability, wherein the additional momentum transfer at the contact line due to the flow in the viscous boundary layer is observed to play a central role.

References

1 P. Brunet, J. Eggers and R. Deegan, *Phys. Rev. Lett.*, 2007, **99**, 144501.
2 J. Boreyko and C.-H. Chen, *Phys. Rev. Lett.*, 2009, **103**, 174502.
3 X. Noblin, A. Buguin and F. Brochard-Wyart, *Phys. Rev. Lett.*, 2005, **94**, 166102.
4 P. Brunet, M. Baudoin, O. B. Matar and F. Zoueshtiagh, *Phys. Rev. E: Stat., Nonlinear, Soft Matter Phys.*, 2010, **81**, 036315.
5 J. R. Friend and L. Y. Yeo, *Rev. Mod. Phys.*, 2011, **83**, 647–704.
6 J. Scortesse, J. Manceau and F. Bastien, *J. Sound Vib.*, 2002, **254**, 927–938.
7 S. Alzuaga, J. Manceau and F. Bastien, *J. Sound Vib.*, 2005, **282**, 151–162.
8 A. Qi, L. Yeo and J. Friend, *Phys. Fluids*, 2008, **20**, 074103.
9 P. M. Morse; K. U. Ingrad. *Theoretical Acoustics*; Princeton University, Princeton, NJ, 1968.
10 M. Lighthill, *Proc. R. Soc. London, Ser. A*, 1952, **211**, 564–587.
11 T. Hasegawa, T. Iizuka, T. Kido and C. Matsuoka, *J. Acoust. Soc. Jpn. (E)*, 2000, **21**, 145–152.
12 B. Chu and R. Apfel, *J. Acoust. Soc. Am.*, 1982, **72**, 1673–1687.
13 R. Beyer, *J. Acoust. Soc. Am.*, 1960, **32**, 719–721.
14 A. Marmur, *Soft Matter*, 2006, **2**, 12–17.
15 S. O'Brien and B. Van den Brule, *J. Chem. Soc., Faraday Trans.*, 1991, **87**, 1579–1583.
16 L. Yeo and H.-C. Chang, *Mod. Phys. Lett. B*, 2005, **19**, 549–569.
17 L. Yeo and H.-C. Chang, *Phys. Rev. E: Stat., Nonlinear, Soft Matter Phys.*, 2006, **73**, 011605.
18 C. Bradley, *J. Acoust. Soc. Am.*, 1996, **100**, 1399–1408.
19 P. de Gennes, *Rev. Mod. Phys.*, 1985, **57**, 827–863.